Rheol Acta (2009) 48:715–733
DOI 10.1007/s00397-009-0364-x

ORIGINAL CONTRIBUTION

# Rheometry for large-particulated fluids: analysis of the ball measuring system and comparison to debris flow rheometry

**M. Schatzmann · G. R. Bezzola · H.-E. Minor · E. J. Windhab · P. Fischer**

Received: 16 March 2009 / Accepted: 12 April 2009 / Published online: 23 April 2009


**Abstract** For large-particulated fluids encountered in natural debris flow, building materials, and sewage treatment, only a few rheometers exist that allow the determination of yield stress and viscosity. In the present investigation, we focus on the rheometrical analysis of the ball measuring system as a suitable tool to measure the rheology of particulated fluids up to grain sizes of 10 mm. The ball measuring system consists of a sphere that is dragged through a sample volume of approximately 0.5 l. Implemented in a standard rheometer, torques exerted on the sphere and the corresponding rotational speeds are recorded within a wide measuring range. In the second part of this investigation, six rheometric devices to determine flow curve and yield stress of fluids containing large particles with maximum grain sizes of 1 to 25 mm are compared, considering both rheological data and application in practical use. The large-scale rheometer of Coussot and Piau, the building material learning viscometer of Wallevik and Gjorv, and the ball measuring system were used for the flow curve determination and a capillary rheometer, the inclined plane test, and the slump test were used for the yield stress determination. For different coarse and concentrated sediment–water mixtures, the flow curves and the yield stresses agree well, except for the capillary rheometer, which exhibits much larger yield stress values. Differences are also noted in the measuring range of the different devices, as well as for the required sample volume that is crucial for application.

**Keywords** Rheometry · Large-particulated fluids · Yield stress fluids · Debris flow material · Ball measuring system · Rheometry comparison · Mud suspension · Sediment water mixture

M. Schatzmann · G. R. Bezzola · H.-E. Minor
Laboratory of Hydraulics,
Hydrology and Glaciology (VAW),
ETH Zürich, 8092 Zürich, Switzerland

E. J. Windhab · P. Fischer (✉)
Institute of Food Science and Nutrition,
ETH Zürich, 8092 Zürich, Switzerland
e-mail: peter.fischer@ilw.agrl.ethz.ch

## Introduction

In many research areas, such as natural hazards (debris flows, avalanches, lavas), building materials (plaster, concrete, paints, etc.), gas and oil industry (soil drilling and evacuation), sewage treatment (pumping slurries), and food industry (yoghurts, sauces, etc.), the rheological behavior of large-particulated fluids containing aggregate particles with grain sizes larger than 0.25 mm must be determined. Although composed of more than one phase, these fluids are often treated as one phase for practical reasons. The determination of rheological data required for, e.g., numerical hazard approximation, scaling, and flow simulation can be an uphill task in particular because of the fluids' multiphase composition and the fact that nonideal viscometer geometries are used to evaluate the flow response of complex fluids (Coussot 2007; Shapley et al. 2004).

A number of rheometers and tests have been developed over the last few decades in order to determine the flow curve or the yield stress of such fluids. For the

determination of flow curves of sediment–water mixtures, large-scale devices were adapted from standard rheometers by Phillips and Davies (1991), Major and Pierson (1992), Coussot and Piau (1995), and Wallevik and Gjorv (1990). In several cases, the inner cylinder of a concentric cylinder system was replaced with rotating blades (Tattersall and Bloomer 1979; Banfill 1994) or impellers (Tattersall and Banfill 1983; Wallevik and Gjorv 1990). Other authors used large capillary (Schulze et al. 1991), inclined plane, or channel geometries for the determination of the flow curve parameters (Coussot and Boyer 1995; Whipple 1997; Parsons et al. 2001). The latter technique is preferably applied for the determination of the yield stress because of the small shear rates applied (Coussot et al. 1996, 1998). The yield stress can be also determined by the slump test, based on either the slump height (for a cylindrical mold Pashias et al. 1996, Ancey and Jorrot 2001 for a conical mold Schowalter and Christensen 1998) or the profile of deposit (Coussot et al. 1996; Roussel and Coussot 2005).

The advantage of these devices is the ability to investigate fluids containing particles larger than 10 mm. On the other hand, the existence of slipping, yield stresses, the approximation of multiphase fluid as a continuous fluid, and the interaction of the rheometer tool with suspended particles may lead to some shortcomings in the description of the viscosity measurements. Other disadvantages include limited ranges of shear rate and shear stress, and the sedimentation of particles over time. Furthermore, experimentation can be very time consuming, especially considering the large sample volumes required (often >100 l) and the need to control concentration and temperature during measurement.

To avoid some of these disadvantages, we use the ball measuring system (BMS) introduced by Müller et al. (1999) to obtain the flow curve and yield stress of large-particulated fluids. Implemented in a standard rheometer (Physica MCR series), the BMS consists of a cylindrical container in which an eccentrically rotating sphere fixed onto a thin holder is dragged through the fluid at defined rotational speeds. To obtain flow curve data, i.e., viscosity data, a relationship between the measured speed $\Omega$ and applied torque $T$, and thus, shear rate $\dot{\gamma}$ and shear stress $\tau$ can be established. Based on the drag characteristics, Tyrach (2001) (see Schatzmann et al. 2003a) derived an approach for the laminar flow regime (sphere Reynolds number $\mathrm{Re} \leq 1$). However, applying this approach for the investigation of clay suspensions (Schatzmann et al. 2003b), deviations of the flow curves obtained with the BMS and a standard Couette geometry were observed in the nonlaminar flow regime ($\mathrm{Re} > 1$). This is because the fluids are non-Newtonian but must been treated as Newtonian, an approximation used in the previous work of Tyrach (2001).

The first part of this manuscript addresses these shortcomings by applying the theory of Metzner and Otto (1957) to describe both the laminar and nonlaminar flow regime of fluids that have shear-thinning, shear-thickening, and yield stress characteristics. The second part compares the performance and reliability of six rheometers and tests used to determine the rheology of large-particulated fluids. This could give a basis for the choice of an appropriate tool for the rheological investigation of large-particle fluids for specific applications.

## Experimental setups and materials

### Rheometry

For the determination of the flow curve, the BMS, the large-scale rheometer (Coussot and Piau 1995), and the building material learning (BML) viscometer were used. For the determination of the yield stress, $\tau_y$, a capillary rheometer, the inclined plane test, and the slump test were used in addition to the mentioned devices.

Implemented in a standard rheometer (Physica MCR series), the BMS consists of a cylindrical container with radius $r_c = 57.5$ mm and height $h_c = 48$ mm where a sample fluid of 0.5 l is introduced. The eccentrically rotating sphere of diameter $D$ is fixed onto a $0.6 \times 3$-mm-thin holder and dragged through the fluid at defined rotational speeds $\Omega$ (Fig. 1). The distance between sphere and container wall is $s_w = 17$ mm, and that between sphere and container bottom is $s_b = 22$ mm. Spheres of variable diameter $D = 8$, 12, and 15 mm were used in the present study. Depending on the sphere diameter $D$, the radius of the center sphere path $r$ and the length of the immerged holder part $s_i$ vary (Table 1).

The large-scale rheometer is described in detail in Coussot and Piau (1995) and shown in Fig. 2. The apparatus is based on a concentric cylinder system with the radius of the outer cylinder $R_o = 585$ mm, the radius of the inner cylinder $R_i = 385$ mm, and a gap between the inner and outer cylinder of $H = 200$ mm. The effective cylinder length is $L = 720$ mm. Accordingly, a very large sample volume of 500 l is required for experimentation. The rotating inner cylinder is driven hydraulically via a combustion engine. Rotational speeds $\Omega$ are measured with a tachometer on the cover of the inner cylinder. The torque $T$ is measured with the

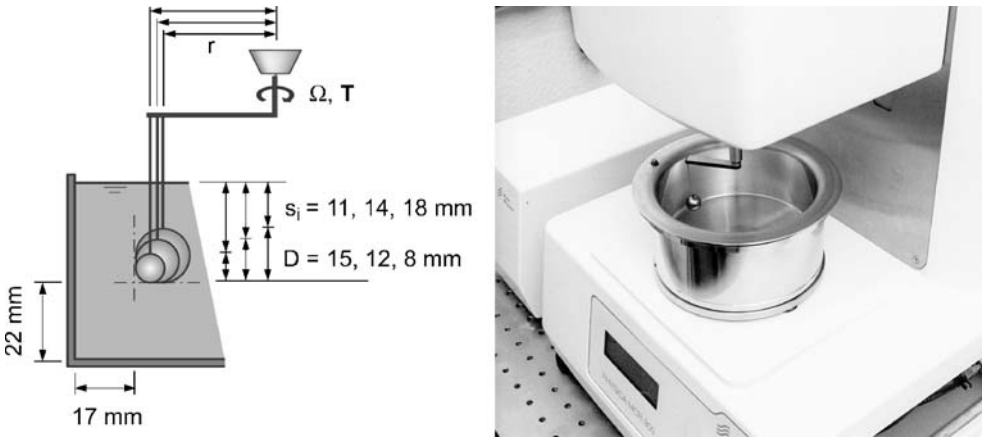


**Fig. 1** The BMS of Müller et al. (1999) implemented in a standard rheometer

help of strain gauges fixed between the inner cylinder and the crankshaft. In order to prevent the test fluid from slipping, steel bars are fixed on the outer cylinder while the inner cylinder surface is covered with a metal mesh. For flow curve experiments, the speed Ω was increased in eight to 10 steps from 0.005 to 0.2 rps. The total torque was measured at each speed step for 120 s with a frequency of 100 Hz (Coussot and Piau 1995; Coussot et al. 1998; Banfill et al. 2000; Ancey 2001). To convert measured $T$ and Ω data into the rheological data shear stress $\tau$ and shear rate $\dot{\gamma}$, the concept of Nguyen and Boger (1987) was applied. The material was partly sheared in the cylinder gap $H$ for each investigated speed Ω. Accordingly the shear rate $\dot{\gamma}_i$ at the periphery of the inner cylinder is:

$$\dot{\gamma}_i = 2\tau_i \frac{d\omega}{d\tau_i}, \tag{1}$$

where $\omega = 2\pi\Omega$ is the angular velocity and $\tau_i$ is the shear stress at the inner cylinder. In order to determine the gradient $d\omega/d\tau_i$, the method of Borgia and Spera (1990) was applied for the conversion of $\tau_i$ and $\omega$ data. For the rheometer, the flow curve was obtained in the range of $1 < \dot{\gamma} < 100\ s^{-1}$ and $200 < \tau < 8{,}000$ Pa. Due to the large sample volume, conducting a flow curve experiment required a total of three person hours to complete experimentation, apparatus cleaning, and determination of the apparatus resistance $T_0$.

The BML viscometer was developed by Wallevik and Gjorv (1990). Today, it is a commercial instrument for testing the rheological properties of concrete (Fig. 3). Based on the principles of a concentric cylinder system, the rotating outer cylinder (radius $R_o$ = 145 mm) is a hollow cylinder with longitudinal ribs in order to avoid wall slip. The inner cylinder ($R_i$ = 100 mm) consists of a tooth-ring-shaped central part with a length of $L$ = 150 mm, which is connected with a load cell in order to measure the required torque. The upper and bottom parts of the inner cylinder are fixed and, thus, separated from this central part, which makes the rheological properties being measured in average fluid depth. The apparatus requires a sample volume of 20 l. The measuring procedure is fully automated and torques are measured at rotational speeds of 0.09 → 0.15 → 0.21 → 0.28 → 0.34 → 0.40 → 0.46 rps. The speed is then decreased and a control measurement is conducted at Ω = 0.31 rps. Each Ω step lasts 6 s. While the first 2 s is required to adjust the speed, the torque is measured in the last 4 s. Sediment–water mixtures containing particles up to $d_{max}$ = 10 and 25-mm grain size were tested with this apparatus. For the conversion of measured into rheological parameters, the concept of Nguyen and Boger (1987) was applied (see Eq. 1) The flow curve was obtained in the range of $10 < \dot{\gamma} < 80\ s^{-1}$ and $20 < \tau < 5{,}000$ Pa. Conducting a flow curve experiment required a total of 15 person minutes for experimentation and apparatus cleaning.

**Table 1** Geometric configuration of the BMS

| Lengths | | | Surface areas | | | Volumes | | |
|---|---|---|---|---|---|---|---|---|
| $D$ (mm) | $r$ (mm) | $s_{im}$ (mm) | Sphere $A_s$ (mm$^2$) | Holder $A_h$ (mm$^2$) | Ratio $A_s/A_h$ (−) | Sphere $V_s$ (mm$^3$) | Holder $V_h$ (mm$^3$) | Ratio $V_s/V_h$ (−) |
| 15 | 33 | 11 | 705.1 | 79.2 | 8.9 | 1767.1 | 19.8 | 89.2 |
| 12 | 34.5 | 14 | 450.6 | 100.8 | 4.5 | 904.8 | 25.2 | 35.9 |
| 8 | 36.5 | 18 | 199.3 | 129.6 | 1.5 | 268.1 | 32.4 | 8.3 |

**Fig. 2** The large-scale concentric cylinder rheometer of Coussot and Piau (1995)

The capillary rheometer used was a large-scale device similar to the one presented by Schulze et al. (1991) that was designed for the yield stress determination of clay dispersions on construction sites. It consists of a vertical cylinder and a horizontal outlet capillary fixed in the bottom region of the cylinder (Fig. 4). While the outlet of the capillary remains closed with a tap, the test fluid is filled in the cylinder up to an initial height close to the top. The capillary is then opened and the fluid flows out, and the level of the fluid in the cylinder thus decreases with time. The outflow stops when a final stagnation level $h_f$ of the fluid in the cylinder is achieved. The vertical cylinder measured 290 mm in diameter and 800 mm in height. Thus, a sample volume of about 50 l is required. The length of the outlet capillary was $L_c = 300$ mm. The diameter of the capillary was varied between $D_c = 38.5, 25$, and 16 mm, depending on the expected yield stress $\tau_y$ of the test fluid. The inside of the capillary was covered with sandpaper. The final stagnation level was measured with the help of a laser distance meter and controlled with a measuring band fixed on the outside of the transparent cylinder. In preliminary experiments, clay suspensions were tested with this apparatus. The end of the experiment was clearly defined by an abrupt change from continuous outflow to a dropping out of the fluid in a much smaller quantity. By contrast, the end of the experiment could not be defined exactly with the different concentrated debris flow material mixtures ($d_{max} = 5$ mm) used in this study because a transition from continuous into interrupted outflow over 20–60 min was observed. During this transition, the outflow became progressively more characteristic of a plug flow. Thus, wall slip must have occurred, which enabled the outflow of the fluid in the end of this transition regime. Slip effects of this kind are a very common phenomenon in capillary rheometry and are usually eliminated or reduced by the use of a rough wall (Nguyen and Boger 1992). The use of sandpaper here was not sufficient to avoid this phenomenon for the debris flow material mixtures. Avoiding this phenomenon by using wall roughness in the order of the grain size of the fluid particles ($d = 1$ to 5 mm) would be technically difficult to realize in capillaries of limited diameter. For the determination

**Fig. 3** The defined BML viscometer used at the concrete consulting company TFB/Wildegg, Switzerland

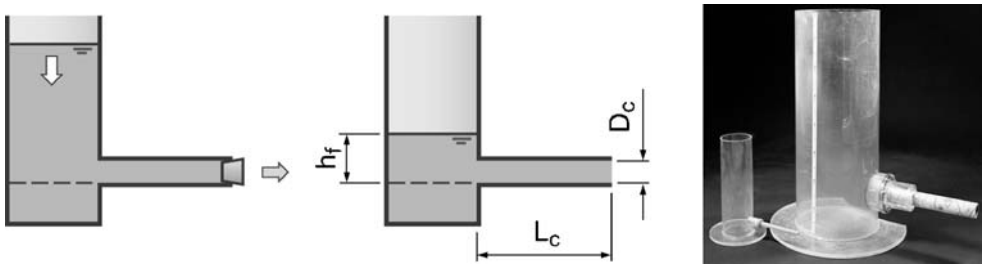


**Fig. 4** Principle and execution of the capillary rheometer

of the yield stress $\tau_y$, the following relation for capillary systems was applied (Chhabra and Richardson 1999):

$$\tau_y = \frac{1}{4}\frac{D_c}{L_c}\rho g h_f, \tag{2}$$

where $\rho$ is the fluid density and $g$ is the acceleration due to gravity. The application of the present apparatus was limited to a yield stress smaller than approximately 300 Pa. For experimentation and apparatus cleaning, 10 min or more was required for an experiment depending on the outflow process of a given fluid across a given capillary.

In the inclined plane test, the fluid is slowly introduced at a fixed location on an inclined plane. Driven by gravity, the fluid spreads downslope, as well as in a lateral direction, finally forming a heap with a specific three-dimensional geometry. Characteristic profiles (deposit depth $h$ against distance $x$ from the deposit border) are obtained depending on the angle $\theta$ (Fig. 5). If a sufficiently large volume is used, the height $h$ of any profile develops a characteristic asymptotic deposition depth $h_0$ at a given distance from the deposition border. The profile of deposit is related to the yield stress of the fluid (Coussot et al. 1996; Wilson and Burgess 1998). In the present study, the test fluids with sample volumes of 50 to 100 l and particles up to $d_{max} = 10$-mm grain size were introduced via a 2.1-m-long polyvinyl chloride (PVC) channel, which was inclined at an angle $i = 5.71°$. The plane was unrestricted in downstream and lateral directions but confined in the backward direction (Fig. 5). The plane surface was made of a uniform granular paint with a surface roughness equivalent to a grain size of $d = 2$ mm. The profile of the deposit was measured in the direction of the highest slope ($\theta = 0°$). Hereby, a thin steel plate was used and the fluid was cut perpendicular to the plane; thus, the profile of the deposit was directly printed on both sides of the plate. The plate was equipped with a coordinate system that enabled the reading of flow depth $h$ as a function of the distance $x$ in increments of 10 mm in the range $0 \le x \le 180$ mm. If the asymptotic deposition depth $h_0$ in the center of the heap is reached, then the yield stress is determined as (Coussot and Boyer 1995):

$$\tau_y = \rho g h_0 \sin(i) \tag{3}$$

In the direction of the highest plane slope ($\theta = 0°$), the following relation between the profile of the deposit and the yield stress $\tau_y$ can be found by the best fitting of $h$ and $x$ data (Liu and Mei 1989; Coussot et al. 1996):

$$\frac{\rho g \sin i}{\tau_y}(x \tan i + h) = -\ln\left|1 - \frac{\rho g h \sin i}{\tau_y}\right| \tag{4}$$

In this study, medium to highly concentrated fluids were tested so that the asymptotic deposition depth $h_0$

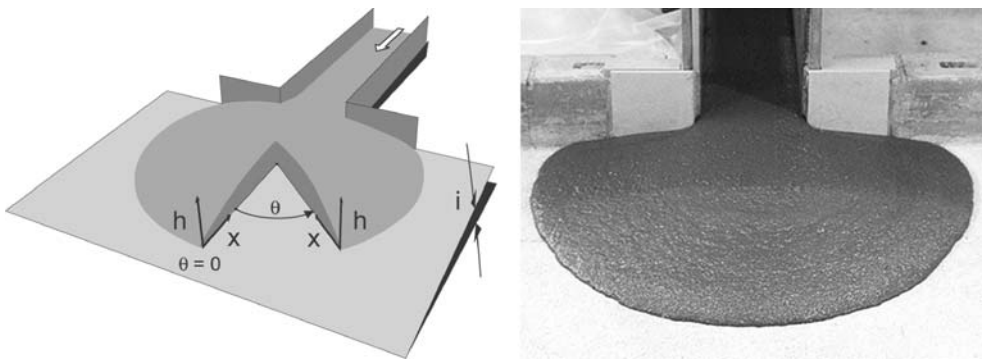


**Fig. 5** Principle and execution of the inclined plane test

was not attained, and thus, only Eq. 4 was applied. The extension of the deposition was much larger than the fluid depth in the heap center $\left(h(x = 180\,\text{mm})/(x = 180\,\text{mm}) \approx 4 - 16\right)$. Thus, the long-wave approximation for which the above equations were proved to be valid was fairly fulfilled. For the considered range of the distance $x$ ($0 \leq x \leq 180$ mm), the measured profile followed the theoretical profile given by Eq. 6 well in all experiments. Respecting the long-wave approximation, the range of the yield stress for which the test can be applied depends on the inclination angle $i$ of the test plane and the sample volume. For the boundary conditions encountered here, the application was limited to approximately $\tau_y \leq 500$ Pa. Conducting one experiment required 45 person minutes for experimentation, measurement, and cleaning of experimental facilities.

For the slump test, a conical or cylindrical container is required, which is open at the top and at the bottom. The container is placed on a horizontal plane and filled with the test fluid up to the container height $H_c$. The container is then suddenly lifted vertically, which allows the fluid to collapse under its own weight. After the fluid comes to rest, two areas can be distinguished: an unyielded center part, which sustained a slump height $S$, and a surrounding yielded part, which spread radially on the test plane (Fig. 6). The yield stress is related either to (a) the slump height $S$, which is the difference between the initial fluid depth (container height $H_c$) before the experiment and the final fluid depth $h_f$ of the unyielded center part after the experiment, or to (b) the profile of the deposit of the yielded/sheared part (deposit depth $h$ against distance $x$ from the deposit border) as for the inclined plane test. A cylindrical PVC container with a height $H_c = 89$ mm and a diameter $D_c = 103.5$ mm was used, which required a sample volume of 0.75 l. At the bottom end of the cylinder, a rubber ring was fixed on the sidewalls in order to avoid eventual drainage of water. The plane was made of PVC and had a smooth surface. The slump height $S$ was determined by measuring the final fluid depth $h_f$ in the center of the deposition and substracting $h_f$ from the cylinder height $H_c$. The profile of the deposit was obtained using a thin steel plate: Cutting the deposit perpendicular to the horizontal plane, the profile was directly printed on the plate. The profile was measured at three different locations (each 120°) along the 360° circle of the radial deposition. The plate was equipped with a coordinate system based on which the flow depth $h$ was measured in function of the distance $x$ from the deposit border in the range $0 \leq x \leq 80$ mm. For a cylindrical container, the yield stress can be calculated based on the slump height $S$ as follows (Pashias et al. 1996):

$$\frac{S}{H_c} = 1 - 2 \cdot \frac{\tau_y}{\rho g H_c}\left(1 - \ln\left(2\frac{\tau_y}{\rho g H_c}\right)\right), \tag{5}$$

where the yield stress is found by iteration. Recently, Roussel and Coussot (2005) proposed a slightly different equation accounting for three-dimensional yieding. We found a good agreement of Eq. 5 with experimental results for the dimensionless slump height $S' = S/H_c$ in the range $0.4 < S' < 0.75$, where the maximum error is ±10%, and therefore, we used the original equation by Pashias et al. (1996). For $S' > 0.75$, no data were tested, and for $S' < 0.4$, the error is larger than ±10%. The yield stress $\tau_y$ can be obtained from the following relation in case of a horizontal plane instead of an inclined plane (Coussot et al. 1996; Ancey and Jorrot 2001):

$$h = \sqrt{\frac{2t_y x}{rg}}, \tag{6}$$

where $\tau_y$ is found by best fitting Eq. 6 on the deposition profile if the long-wave approximation is adequate. For the mixtures where Eq. 6 was applied, the deposition diameter outweighed the center height by a factor 8 to 40, which means that the long-wave approximation should be accurate. For the range of the distance $x$ from the border ($0 \leq x \leq 80$ mm), the measured profile did not follow the theoretical profile of Eq. 6, in contrast to the inclined plane test. At the deposition

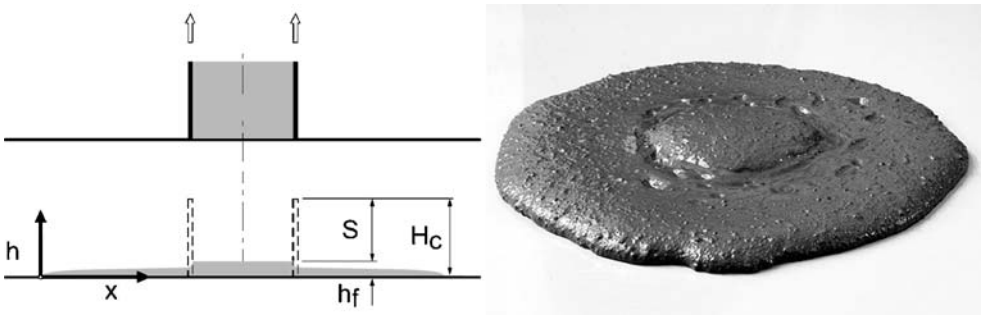


**Fig. 6** Principle and execution of the slump test

border, the increase of the depth $h$ was larger than predicted. By contrast, the increase of the depth $h$ was smaller than predicted for distances $x$ from the border longer than about 30 mm. This phenomenon is almost negligible in highly concentrated mixtures but predominantly observed in less concentrated mixtures. From Baudez et al. (2002), it is known that the plane surface roughness does not influence the slump height $S$ of the unyielded central part. However, the influence of roughness on the profile of deposit has not been investigated yet. It is therefore assumed that, due to the smooth plane surface, the spreading fluid is not only sheared but partially slides on the horizontal plane. This could alter the deposition behavior and, thus, result in a different profile of the deposit. With the used cylinder device, the yield stress was determined for $\tau_y < 60$ Pa based on the profile of the deposit and for $40 < \tau_y < 600$ Pa based on the slump $S$. Conducting one experiment required 15 person minutes, including fluid filling, experimental, measuring, and cleaning time.

### Test fluids

Different Newtonian, power law, and fine-particulated yield stress fluids were investigated in a standard measuring system (cone-plane or concentric cylinder system) and the BMS. These fluids were used for the flow analysis of the BMS. Large-particulated yield stress fluids were investigated in the comparison of the six rheometers and to assess the limits of the BMS concerning the use of the maximum grain size.

As Newtonian fluids, six silicon oils with the viscosities $\eta = 0.0514$, 1.01, 2.03, 13, 30.2, and 61.8 Pa·s (AK 50, 1,000, 2,000, 12,500, 30,000, and 60,000; Wacker Chemie, Burghausen, Germany) were used. Four different aqueous carbomethylcellulose (CMC, Fluka, Buchs, Switzerland) and guar gum solutions (Meyprodor 400, Rhodia, Zaandam, Netherlands) were used as power law fluids. Volumetric concentrations of $C_v = 0.01$ (1%) and 0.02 (2%) result in zero shear viscosities $\eta_0 = 7$, 15, 150, 250 Pa·s. Here, $C_v$ is calculated as follows: $C_v = V_s/(V_s + V_w)$, with $V_s$ = volume of the solids and $V_w$ = volume of the added water.

As fine-particulated yield stress fluids, three sediment–water mixtures of medium to high sediment concentration $C_v$ made of natural debris flow material and of four clay dispersions of low to medium sediment concentration $C_v$ were tested. The maximum grain size in both fluids was $d_{max} = 0.25$ mm. The grain material of the natural debris flow sediment–water mixtures was taken from a fresh deposit of a viscous debris flow in the Maschänserrüfe torrent near Trimmis, Switzerland (Schatzmann 2005). The grain material of the clay dispersions is a commercially available natural material (Opalinus clay) used in construction for sealing purposes.

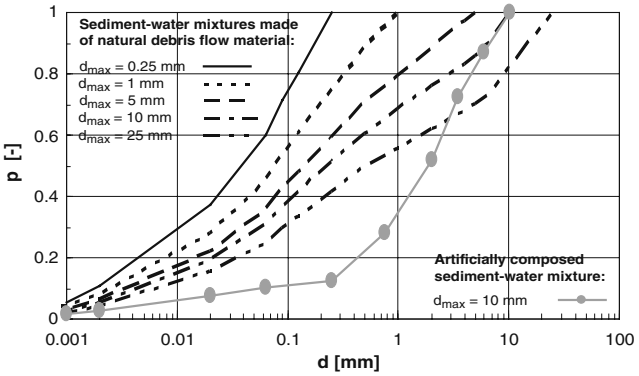


**Fig. 7** Grain size distribution of sediment–water mixtures made from natural debris-flow material and artificial composition

Large-particulated yield stress fluids, i.e., sediment–water mixtures, were made of natural debris flow material with different maximum grain sizes $d_{max}$ and different sediment concentrations $C_v$. One artificially composed sediment–water mixture with a maximum grain size $d_{max} = 10$ mm was tested as reference. For the natural debris flow material, portions of different maximum grain size $d_{max}$ ($d_{max} = 25$ mm, $d_{max} = 10$ mm, $d_{max} = 5$ mm, $d_{max} = 1$ mm, $d_{max} = 0.25$ mm) were sieved from the complete grain material of a deposit of a viscous debris flow in the Maschänserrüfe torrent near Trimmis, Switzerland (Schatzmann 2005). The full grain size distribution of the material that includes sediments from the clay up to the boulder fraction is shown in Fig. 7. The different portions were then mixed with rain water (pH 4.7) in order to obtain sediment–water mixtures with medium to high sediment concentrations $C_v$, for which particle settling was negligible. For the artificially composed sediment–water mixture, sand and rounded gravel was added to the same grain material (clay, silt, and fine sand) already used for the clay dispersion. The sediments were mixed with tap water (pH 6.5) in order to obtain a highly viscous mixture with a sediment concentration of $C_v = 0.683$. Temperature was kept constant at $20° \pm 1°$ during all tests.

## Data conversion for the BMS

The objective of this section is to establish a relation based on the principles of Metzner and Otto (1957) between the drag flow around the sphere and the classic shear flow in order to convert the measured parameters

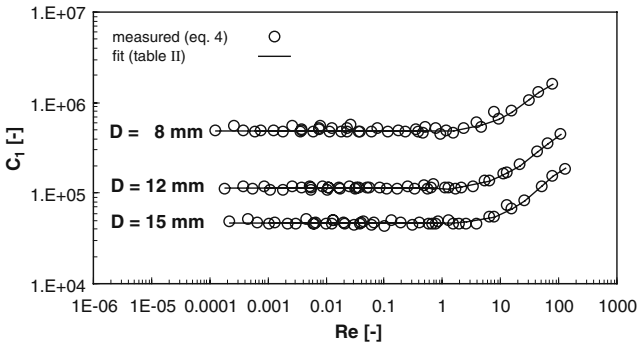


**Fig. 8** Relation between the system number $C_1$ and the Reynolds number Re for the BMS spheres with the diameter $D = 8$, 12, 15 mm using silicon oils with viscosity $\eta = 0.05$, 1, 2, 12.5, 30, 60 Pa·s

$\Omega$ and $T$ into rheological parameters, i.e., shear rate $\dot{\gamma}$ and shear stress $\tau$. The power characteristic of the Metzener and Otto approach is used for the derivation of the relationship between the shear rate $\dot{\gamma}$ and the rotational speed $\Omega$. Once this relationship is known, the relationship between the shear stress $\tau$ and the torque $T$ can be derived. In the present study, the conversion was derived for a laminar flow around the sphere (Re $\leq$ 1), as well as for the transitional regime (1 < Re < 100).

## Power characteristic and determination of the BMS system number $C_1$

The power $P$ of a stirring system at a constant rotational speed $\Omega$ is:

$$P = 2\pi T\Omega \tag{7}$$

The dimensionless power number (Newton number) Ne is described as follows (Metzner and Otto 1957):

$$\mathrm{Ne} = \frac{P}{\Omega^3 D^5 \rho} = \frac{2\pi T}{\Omega^2 D^5 \rho}, \tag{8}$$

where $D$ is the sphere diameter and $\rho$ is the fluid density. The sphere Reynolds number Re is:

$$\mathrm{Re} = 2\pi \frac{\Omega r D \rho}{\eta}, \tag{9}$$

where $r$ is the radius of the center sphere path and $\eta$ is the viscosity. Multiplying the power number (Eq. 8) with the Reynolds number (Eq. 9), a characteristic BMS system number $C_1$ is obtained:

$$C_1 = \mathrm{ReNe} = 4\pi^2 \frac{rT}{\eta\Omega D^4} \tag{10}$$

In the present study, $C_1$ was determined with the help of different Newtonian silicon oils ($\eta$ = const.) measured in the BMS and referenced in a cone and plate or a concentric cylinder system. $C_1$ turned out to be constant for Re $\leq$ 1, but it increased for Re > 1 (Fig. 8). The increase of $C_1$ is probably due to wake formation and the onset of turbulence in the transitional regime (Clift et al. 1978). For Re $\leq$ 1, an average value of $C_1$ was determined based on the set of $C_1$ and Re data. For Re > 1, a polynomial function was fitted to the $C_1$ and Re data (Table 2).

## Determination of the relation between the shear rate $\dot{\gamma}$ and the speed $\Omega$

Power law fluids are used for the derivation of the shear rate $\dot{\gamma}$ based on the power characteristics of the measuring system. The viscosity $\eta$ of a power law fluid is:

$$\eta = m\dot{\gamma}^{n-1}, \tag{11}$$

where $m$ is the power law consistency coefficient and $n$ is the power law index. Further, Eq. 10 can be transformed into an expression for the viscosity:

$$\eta = 4\pi^2 \frac{rT}{\Omega D^4 C_1} \tag{12}$$

With Eq. 11 introduced in Eq. 12, the following expression for the shear rate $\dot{\gamma}$ is found:

$$\dot{\gamma} = \left(4\pi^2 \frac{rT}{m\Omega D^4 C_1}\right)^{\frac{1}{n-1}} \tag{13}$$

CMC–water solution (1% CMC solution) and a guar–water solution (1% guar solution) were used as power law fluid. Based on reference measurements in the concentric cylinder system, the consistency coefficient

**Table 2** Value or function of the system number $C_1$ depending on the range of the sphere Reynolds number Re for the different BMS sphere sizes $D$

| $D$ (mm) | Re $\leq$ 1: $C_1$ = const. | Re > 1: $C_1 = \sum_{j=0}^{j=4} a_j \cdot \mathrm{Re}^j$ | | | | |
|---|---|---|---|---|---|---|
| | $C_1$ (−) | $a_0$ (−) | $a_1$ (−) | $a_2$ (−) | $a_3$ (−) | $a_4$ (−) |
| 15 | 46,775.9 | 4.44E+04 | 1,308.4 | 5.8868 | −0.077994 | 0.00014926 |
| 12 | 113,384.6 | 1.05E+05 | 4,843.6 | −20.678 | 0.065062 | −0.00024068 |
| 8 | 491,381.6 | 4.60E+05 | 20,743 | 87.252 | −4.9636 | 0.036844 |

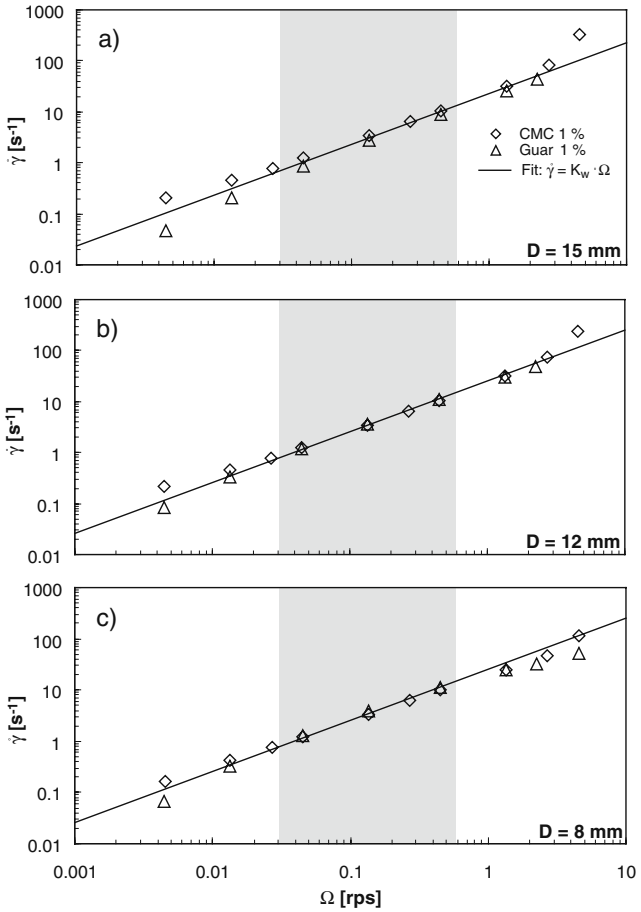


**Fig. 9** Relation between the shear rate $\dot{\gamma}$ and the rotational speed Ω for the BMS spheres with the diameter $D = 8, 12, 15$ mm (power law fluids) (**a**–**c**)

$m$ and the index $n$ were determined by fitting a power law model function to the flow curve data. The same fluids were then investigated in the BMS where the torque was measured for the different specified speeds. Using the system number $C_1$ given in Table 2, the shear rates were then calculated using Eq. 13.

It must be noted that the value of $C_1$ is a priori unknown for the used power law fluid, because the Reynolds number for a given speed is not known. The adapted Reynolds number for power law fluid defined by Atapattu et al. (1995) was therefore used for the first estimation. The shear rate is then calculated according to Eq. 13 and $\eta$ calculated based on the flow curve/viscosity curve function of the reference measurements. The Reynolds number is then recalculated with Eq. 9. For recalculated Reynolds numbers smaller than 1, procedure stops because $C_1$ is constant. For recalculated Reynolds numbers, Re larger than 1, $C_1$, $\dot{\gamma}$, $\eta$, and Re are calculated in several rounds (iterations) until the calculated values converge.

After this procedure, the shear rate data are plotted vs the rotational speed (Fig. 9). For all three spheres, the shear rates obtained with both power law fluids slightly diverge at low speeds ($\Omega < 0.03$ rps). For rotational speeds $\Omega > 0.03$ rps, data of both fluids correspond well. At elevated speeds of $\Omega > 2$ rps, corresponding to Reynolds numbers Re > 1–20, data of both fluids deviate from this linearity. For the smallest sphere ($D = 8$ mm), data deviate from linearity already for $\Omega > 1$ rps, which corresponds to Re > 1 (Fig. 9a). The divergence is due to elastic behavior of both polymers that is different for the investigated CMC and guar solutions. For further calculation, therefore, only rotational speeds $\Omega > 0.03$ rps are used. To avoid possible influence of nonlaminar flow behavior, only data within laminar flow (Re < 1) are considered. In this range, $\Omega > 0.03$ rps and Re < 1 (which approximately corresponds with $\Omega < 0.6$ rps), a linear relation between $\dot{\gamma}$ and Ω is found:

$$\dot{\gamma} = K_\Omega \Omega \tag{14}$$

The average coefficient $K\Omega$ and the standard deviation were calculated based on the corresponding set of $\dot{\gamma}$ and Ω data for each sphere (Table 3).

## Determination of the relation between the shear stress $\tau$ and the torque $T$

The relation between $\tau$ and $T$ was investigated for Newtonian, power law, and yield stress fluids. In the latter case, only sediment–water mixtures containing particles smaller than $d_{max} = 0.25$ mm were used. All fluids were investigated in both the standard measuring system (cone and plane or concentric cylinder system) using the Rheometric Scientific DSR rheometer and the BMS. The flow curve in the standard measuring system and the $T(\Omega)$ relationship in the BMS were determined. The obtained flow curve was then fitted to the appropriate model functions and, finally, the shear stress $\tau$ was calculated for the reference fluids and BMS-shear rates based on the data obtained from the DSR.

**Table 3** Constant $K\Omega$ relating the rotational speed Ω with the shear rate $\dot{\gamma}$ and standard deviation $\sigma K\Omega$ of the constant $K\Omega$ for the different BMS spheres $D$

| $D$ (mm) | $K\Omega$ (−) | $\sigma K\Omega$ (%) |
|---|---|---|
| 15 | 22.8 | 12.3 |
| 12 | 25.6 | 6.6 |
| 8 | 25.6 | 10.6 |

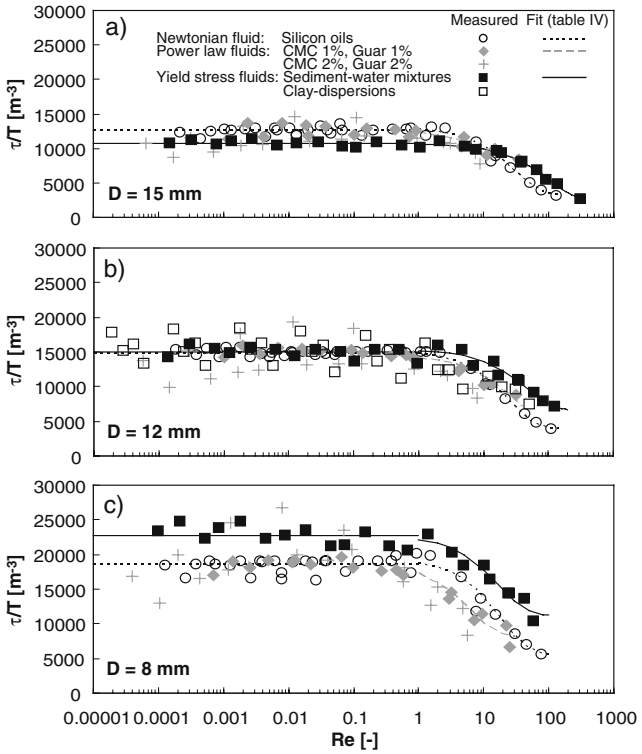


**Fig. 10** Relation between the ratio of shear stress and torque $\tau/T$ and the sphere Reynolds number Re for different types of fluids and different BMS spheres $D = 15, 12, 8$ mm (**a**–**c**)

Analyzing calculated shear stresses against measured torques, a linear relationship between the two parameters resulted for Re $\leq 1$ over the entire range of the torque, while data for Re $> 1$ deviated from this linearity. Therefore, the relation between $\tau$ and $T$ was derived as a function of the Reynolds number Re. The relation between the ratio $\tau/T$ and Re is shown in Fig. 10 for the different BMS spheres: For a given sphere and a given fluid group, the ratio $\tau/T$ is constant in the laminar flow regime (Re $\leq 1$). In the transitional regime (Re $> 1$), $\tau/T$ decreases. For the concentrated power law fluids (2% CMC and 2% guar solution), no clear relationship was deduced either in the laminar or in the transitional regime. This is most probably due to elasticity present in these fluids.

In the next step, $\tau/T$ and Re data of each fluid group were fitted with specific functions depending on the flow regime. For the laminar flow regime (Re $\leq 1$), it is:

$$\tau = K_T T \tag{15a}$$

For the transitional regime (Re $> 1$), the relation can be well described with the following function:

$$\tau = \left[k_1 + k_2 e^{(-k_3 \cdot Re)}\right] T \tag{15b}$$

The average value of the coefficient $K_T$ of Eq. 15a, as well as the coefficients $k_1$, $k_2$, and $k_3$ of Eq. 15b, were calculated based on the corresponding $\tau/T$ data set for each sphere and each fluid group using the least-squares method. All coefficients and their standard errors are listed in Table 4. In order to obtain dimensionless

**Table 4** Coefficients $K_T$ ($K'_T$) and $k_j$ and standard error $\sigma K_T$, $\sigma K'_T$, $\sigma k_j$ for the conversion of the measured torque $T$ into the shear stress $\tau$

| Re $\leq 1$ | Newtonian fluids and power law fluids 1[a] | | | Yield Stress Fluids 1[b] | | | |
|---|---|---|---|---|---|---|---|
| $D$(mm) | $K_T$(m$^{-3}$) | $K'_T$ (−) | $\sigma K_T(\sigma K'_T)$ (%) | $K_T$(m$^{-3}$) | $K'_T$ (−) | $\sigma K_T(\sigma K'_T)$ (%) | |
| 15 | 12,600 | 0.3261 | 3.8 | 10,700 | 0.2769 | 3.5 | |
| 12 | 14,900 | 0.2834 | 3.2 | 15,000 | 0.2853 | 4.5 | |
| 8 | 18,500 | 0.2221 | 2.9 | 22,800 | 0.2737 | 5.4 | |
| Re $> 1$: | $D$ (mm) | $k_1$ (m$^{-3}$) | $k_2$ (m$^{-3}$) | $k_3$ (−) | $\sigma k_1$ (%) | $\sigma k_2$ (%) | $\sigma k_3$ (%) |
| Newtonian fluids | 15 | 3,094 | 10,052 | 0.033435 | 10.5 | 3.3 | 9.9 |
| | 12 | 3,975 | 11,379 | 0.043100 | 7.1 | 2.6 | 7.9 |
| | 8 | 5,553 | 13,910 | 0.052913 | 13.7 | 5.7 | 16.5 |
| Power law fluids 1 | 15 | 8,513 | 4,254 | 0.115740 | 9.4 | 20.7 | 51.8 |
| | 12 | 4,927 | 9,440 | 0.036701 | 126.9 | 62.8 | 109.9 |
| | 8 | 8,068 | 10,873 | 0.167510 | 14.3 | 13.1 | 34.6 |
| Yield stress fluids 1 | 15 | 2,293 | 8,377 | 0.009679 | 17.2 | 4.6 | 10.3 |
| | 12 | 6,603 | 8,790 | 0.021948 | 15.2 | 10.8 | 27.0 |
| | 8 | 11,172 | 11,635 | 0.055850 | 10.4 | 9.8 | 27.0 |

[a]Polymers 1% (CMC 1% and Guar 1%)
[b]Sediment–water mixtures made of natural debris flow material

values, the coefficients are multiplied with the radius of the center sphere path $r$ and the total of sphere surface $A_s$ and sphere holder surface $A_h$ (see specific values in Table 1). The dimensionless constant $K'_T$ is then given by:

$$K'_T = K_T r(A_s + A_h) \tag{16}$$

## Application of the BMS approach to large-particulated yield stress fluids

Sediment–water mixtures made of natural debris flow material with variable maximum grain size ($d_{max} = 1, 5, 7, 10$ mm) and sediment concentration $C_v$, as well as one artificially composed sediment–water mixture ($d_{max} = 10$ mm, $C_v = 0.683$), were investigated with the BMS using different sphere sizes. The flow curve data of the different mixtures are shown in Fig. 11. For the mixtures containing particles up to $d_{max} = 1, 5, 7$ mm grain size, almost identical flow curves are obtained with the different sphere sizes (Fig. 11a–c). A tendency is indicated where the smaller spheres provide flow curves on a slightly higher level of the shear stress $\tau$ compared to the larger spheres. This tendency is most obvious in the mixtures containing particles up to $d_{max} = 10$ mm grain size (Fig. 11d). Both smaller spheres ($D = 8$, 12 mm) exhibit shear stresses, which are approximately 30% to 40% larger than the shear stresses obtained with the largest sphere ($D = 15$ mm) as far as the sediment–water mixtures made of debris flow material are concerned (Fig. 11d). For the highly concentrated, artificially composed sediment–water mixture (Fig. 12), the smallest sphere ($D = 8$ mm) exhibits shear stresses that are approximately 75% larger, and the medium sphere ($D = 12$ mm) exhibits shear stresses that are approximately 20% larger compared to the shear stresses obtained with the largest sphere ($D = 15$ mm). Additionally, the differences in the value of the shear stress for the different spheres are amplified for high shear rates or high Reynolds numbers. The results obtained after data fitting can be summarized as follows:

### Laminar flow regime (Re ≤ 1)

The Newtonian fluids and power law fluids had identical coefficients $K_T$ for a given BMS sphere, whereas the $K_T$ values obtained for the sediment–water mixtures (yield stress fluid) are slightly higher (Fig. 10, Table 4). It is postulated that this is due to the presence of a yield stress in these types of fluids. This hypothesis is verified

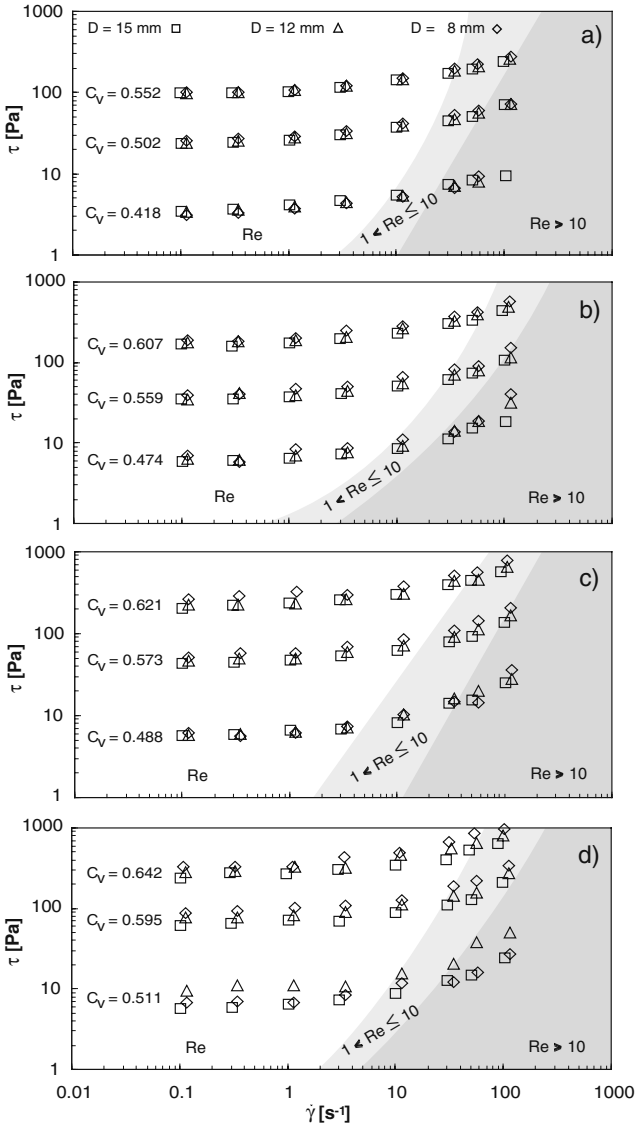


**Fig. 11** Flow curves of sediment–water mixtures made of natural debris flow material with different maximum grain sizes $d_{max}$ and variable sediment concentrations $C_v$. **a** $d_{max} = 1$ mm, **b** $d_{max} = 5$ mm, **c** $d_{max} = 7$ mm, **d** $d_{max} = 10$ mm. Comparison of results for the BMS spheres with the diameter $D = 8, 12, 15$ mm

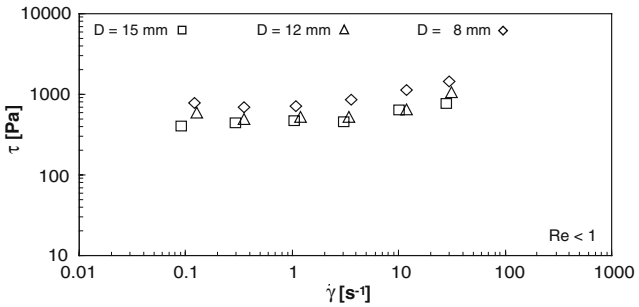


**Fig. 12** Flow curve of artificial sediment–water mixture with maximum grain size $d_{max} = 10$ mm and sediment concentration $C_v = 0.683$. Comparison of results for the BMS spheres with the diameter $D = 8, 12, 15$ mm

later with the help of the yield stress criterion. The clay dispersions (yield stress fluids) were investigated with the 12-mm BMS sphere, and the same value of the coefficient $K_T$ was obtained ($K_T = 15{,}300\ \mathrm{m}^{-3}$) as the one obtained for the sediment–water mixtures ($K_T = 15{,}000\ \mathrm{m}^{-3}$), which are made of natural debris flow material. By comparison, data scatter around this average value is considerably higher compared to the sediment–water mixtures (Fig. 10, $D = 12$ mm). This larger data scatter is due to the fact that the clay dispersions have a slight thixotropy character (Schatzmann et al. 2003a).

### Transitional regime (Re > 1)

Depending on the type of fluid, there is a specific relation between the ratio $\tau/T$ and the Reynolds number. Up to a critical Re, $\tau/T$ is constant and drops as $\mathrm{Re}_{\mathrm{crit}}$ is exceeded. $\tau/T$ for the Newtonian fluids decreases much earlier with increasing Re than for the yield stress fluids. The power law fluids leave the constant $\tau/T$ ratio already for Re > 0.1. The $\tau/T$ data obtained for the clay dispersions (yield stress fluid) indicate another relationship apart from that of the $\tau/T$ data obtained for the sediment–water mixtures made of natural debris flow material (yield stress fluid). It is assumed that this different behavior is due to thixotropic effects of the clay dispersions.

The reference fluids considered for a given type of fluid did not always indicate a unique relationship of the $\tau/T$ ratio vs the Reynolds number. This was specifically apparent in the case of the yield stress fluids, where the clay dispersions showed a different behavior from the sediment–water mixtures made of debris flow material. At this stage, it remains open if this is due to thixotropy of the clay dispersions. It is important that the empirical coefficients derived in this regime for the different types of fluids must be regarded as first-estimation coefficients that must be tested and improved in the future with further fluids.

### Reliability of data conversion: the yield stress criterion

An important control to prove the reliability of the data conversion in the laminar flow regime (Re < 1) for the yield stress fluids is to investigate whether the yield stress criterion is fulfilled or not. In a system where a sphere is dragged across a yield stress fluid, the following dimensionless yield stress number $Y$ was formulated by Beris et al. (1985) in order to express the onset of motion:

$$Y = \frac{1}{2}\frac{\tau_y A_s}{F}, \tag{17}$$

where $\tau_y$ is the yield stress, $A_s$ is the area of the sphere surface, and $F$ is the applied force. For the BMS, the following relationship was found in the laminar flow regime based on Eq. 15a and 16 of the present study:

$$\frac{\tau}{T} = K_T = \frac{K'_T}{r\,(A_s + A_h)} \tag{18}$$

Here, the area of the sphere holder surface $A_h$ appears beside the area of the sphere surface $A_s$. This is because the drag flow is exerted on both the sphere and the sphere holder. Replacing the torque and the radius $r$ of the center sphere path by the force $F(= T/r)$, Eq. 18 is rewritten as:

$$K'_T = \frac{\tau\,(A_s + A_h)}{F} \tag{19}$$

For creeping flow (Re << 1), $\tau$ may be replaced by the yield stress $\tau_y$. Comparing Eq. 19 with Eq. 17 under the condition of creeping flow, it can be concluded that:

$$K'_T \approx 2Y \tag{20}$$

It is most important that, in the case of the critical state between motion and no motion, $K'_T$ or $Y$ should take a specific value, independent of the sphere size and independent of the investigated yield stress fluid. Regarding the $K'_T$ values obtained in the BMS for the yield stress fluids (Table 4), $K'_T$ roughly takes the same value for all three spheres. Given that the $K'_T$ values are included in the empirical formula for the conversion of measured data into rheological data, it can be concluded that the derived approach fulfills the yield stress criterion. It must be noted here that the earlier approach of Tyrach (2001) did not fulfill the yield stress criterion because the $K'_T$ values obtained for the three spheres varied widely (Schatzmann 2005). This is because the particular behavior of yield stress fluids in the conversion of the torque into the shear stress was not considered.

Comparing in a second step the $Y$ value of the present study with the same value obtained by other authors, the BMS value of $Y \sim 0.14$ ($K'_T \sim 0.28$) corresponds fairly well with the value of $0.18 \pm 0.06$ obtained by the observation on the motion/no motion of spheres under freefall conditions and the observation of the residual force upon the cessation of the flow (Ansley and Smith 1967; Chhabra and Richardson 1999). It is further in line with the value of 0.143 obtained by numerical simulations of the onset of motion of spheres in yield stress fluids (Beris et al. 1985; Beaulne and Mitsoulis 1997; Blackery and Mitsoulis 1997; Tabuteau et al. 2007).

## Comparison of rheometrical devices for debris flow material

In order to determine the flow curve and yield stress of large-particle fluids with variable maximum grain sizes $1 < d_{max} < 25$ mm, the large-scale rheometer of Coussot and Piau, the BML viscometer, the BMS, a capillary rheometer, the inclined plane test, and the slump test were compared.

### Flow curve

In Fig. 13, the comparison of the stress readings for all tested rheometers at different solid concentrations $C_v$ is presented. While the BML viscometer provides one flow curve for a given fluid, the BMS and the large-scale rheometer of Coussot and Piau provide a flow curve range or a stress range. For the BMS, the flow curve range is obtained through the use of different sphere sizes. All three measuring systems exhibit flow curves that are in the same range of shear stresses, except for the medium concentrated debris flow material mixture, where the stress range of the large-scale rheometer is on a higher level (Fig. 13a). It is assumed that the apparatus resistance torque $T_0$ was higher during the measurement of this specific mixture than in the other cases. A stress range is indicated only when the measurements of the latter apparatus showed either no dependence on the torque and speed data (Fig. 13a) or showed a hysteresis between the up and down curves (Fig. 13d).

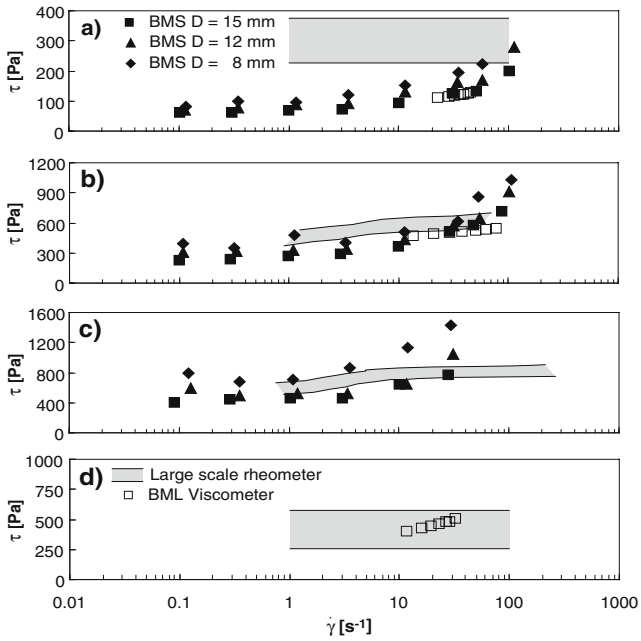


**Fig. 13** Comparison of flow curves of various sediment–water mixtures using different rheometers: **a** Debris flow material mixture with maximum grain sizes $d_{max} = 10$ mm and sediment concentrations $C_v = 0.595$, **b** debris flow material mixture with $d_{max} = 10$ mm and $C_v = 0.642$, **c** artificial mixture with $d_{max} = 10$ mm and $C_v = 0.683$, **d** debris flow material mixture with $d_{max} = 25$ mm and $C_v = 0.643$

The shape of the flow curve resulting from the different rheometers is not identical. For higher shear rates ($\dot{\gamma} \geq 10$–$50$ s$^{-1}$) the BMS provides a stronger stress increase compared to the other systems. This range corresponds with the beginning of the transitional regime of the measuring sphere ($1 < Re < 15$). Considering the discussion of the previous section, it is possible that the conversion of BMS data into rheological data derived for fine-particle fluids is different for large-particle fluids. However, it is more likely that particle segregation in the shear gap of the large-scale rheometer and BML viscometer occurs that leads to a reduced stress increase.

It is noticeable that the smaller BMS spheres displayed a tendency to have flow curves on a larger shear stress level than the larger spheres. This phenomenon was found in the coarsest mixtures ($d_{max} = 10$ mm) and was most dominant for very high sediment concentrations $C_v$ (Fig. 13c), whereas it did not appear or was negligible for mixtures containing smaller particles ($d_{max} \leq 5$ mm) (Schatzmann 2005). The phenomenon is thus related to the fact that the sphere holder of the smaller spheres is longer and closer to the container wall compared to the larger spheres. This enhances the probability for temporary blockage and jamming effects, especially in the coarser and highly concentrated mixtures using smaller, compared to larger, spheres.

### Yield stress

The general Herschel–Bulkley model was fitted to the flow curve data of the different mixtures in order to calculate the yield stress $\tau_y$. For the BML viscometer, an exact determination of the yield stress was impossible due to the lack of shear stress data at low and medium shear rates $\dot{\gamma} < 10$ s$^{-1}$. Therefore, the yield stress $\tau_y$ was additionally estimated based on the coefficient $a_0$ ($\tau_y \approx a_0$) used for the conversion of the $\tau$ and $\Omega$ data according to Borgia and Spera (1990), which was also proposed earlier by Major and Pierson (1992). For all other tests (capillary rheometer, inclined plane test, and slump test) the yield stress was determined based on Eq. 2.

Overall, a fairly good agreement of the yield stress of particulated fluids of different $d_{max}$ was found for the slump test, the inclined plane test, the BML viscometer,

the BMS, and the large-scale rheometer (Fig. 14): For 16 out of 19 mixtures, the yield stress deviates less than 30% from the values obtained by the medium BMS sphere $D = 12$ mm. For three mixtures, the deviation is between 30% and 50% (BML viscometer, slump test/profile of deposit). Within the comparison, the values of the BML viscometer are higher (+20%), whereas the values of the inclined plane test and the slump test are slightly lower (−5%) than the values of the medium BMS sphere. The large-scale rheometer provides $\tau_y$ values that are, on average, 25% higher (variation between −20% and +80%) than the values of the BMS sphere $D = 12$ mm.

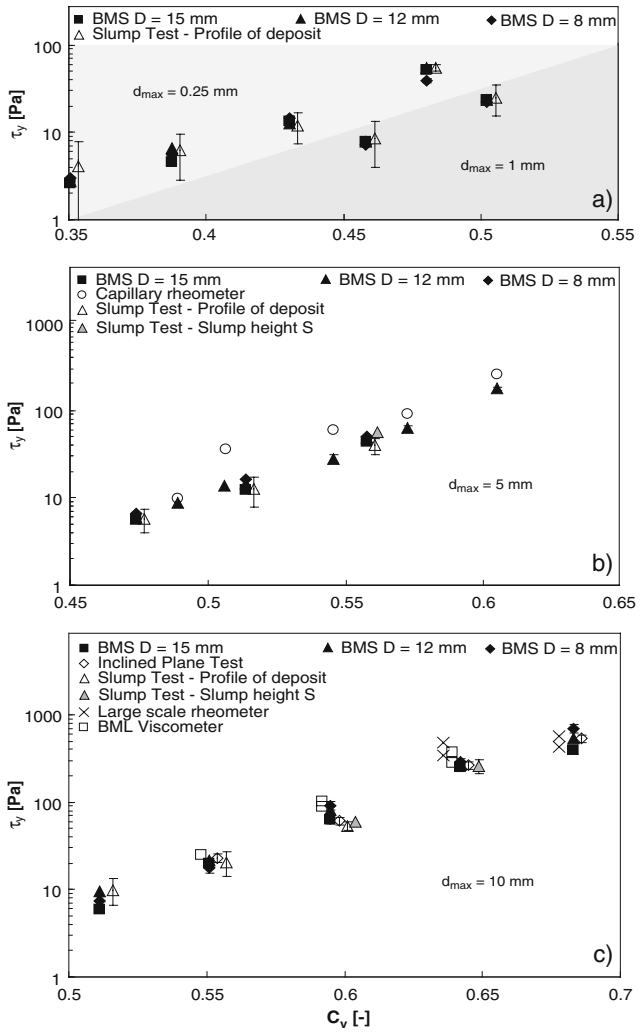


**Fig. 14** Comparison of the yield stress $\tau_y$ of debris flow material mixtures from different rheometers and tests: **a** maximum grain sizes $d_{max} = 0.25$ and 1 mm for variable sediment concentrations $C_v$, **b** maximum grain sizes $d_{max} = 5$ mm for variable sediment concentrations $C_v$, **c** maximum grain size $d_{max} = 10$ mm for variable sediment concentrations $C_v$

The capillary rheometer exhibits $\tau_y$ values that are, on average, 75% (variation between +15% and +160%) higher than the comparable values of the BMS (Fig. 14a). This large difference cannot be explained solely by the uncertain definition about the end of the experiment, which was the case for the debris flow material mixtures, because roughly the same difference in the $\tau_y$ value was also noted in case of clay suspensions, where the end of the experiment was clearly defined.

Since a reduced capillary length $L'_c = L_c - 2D_c$ instead of the real capillary length $L_c$ in Eq. 2, as proposed by Schulze et al. (1991), leads to an even higher $\tau_y$ value, we assume that the flow from the vertical cylinder into the capillary must be partly disturbed or accompanied by an additional resistance, which is not yet considered in Eq. 2. Blockage of the capillary entrance by larger particles is not assumed to be the reason for the additional resistance because the difference of $\tau_y$ value was obtained in both debris flow material mixtures containing particles up to $d_{max} = 5$ mm grain size and clay dispersions containing particles up to $d_{max} = 0.25$ mm grain size only. Future work should thus clarify the exact reason for this difference of the yield stress obtained with the capillary rheometer. In case of the lowest concentrated debris flow material mixture (Fig. 14a; $C_v = 0.488$), where the yield stress only differed by +15%, a second effect occurred, which balanced the unknown first effect: Particle settling on the cylinder ground took place during the rather long experimental phase. Hence, a less concentrated mixture, not the representative, with an altered grain size distribution, flew across and stopped in the outflow capillary. The yield stress of this more liquid mixture is evidently lower than the yield stress of the real mixture.

## Application notes and suggestions

The large-scale rheometer and the BML viscometer allow the determination of the flow curve of fluids having $d_{max} = 25$ mm, while the BMS in its present configuration is restricted to fluids having $d_{max} = 10$ mm. Due to the large apparatus resistance $T_0$, the large-scale rheometer yields useful rheological data only for concentrated fluids. The BML viscometer allows measurements for medium to highly concentrated fluids, while the BMS principally allows measurements for the entire range of concentration or shear stresses. Due to its implementation in a standard rheometer, rheological data can be obtained for low to high shear rates with the BMS, whereas the application of the large-scale rheometer is restricted to medium to high shear rates and the BML viscometer to a relatively small range of high shear rates only.

When working with the large-scale rheometer, the main burden is the very large sample volume of 500 l required for experimentation. Preparation of such a volume is intensive and usually takes one to several hours, depending on the sample fluid composition. Likewise, the experimentation is intensive. Accurate control of the sediment concentration $C_v$ (in case of sediment–water mixtures) and fluid temperature remains difficult. With the BML viscometer, the required sample volume of 20 l can be prepared and managed, and experiments can be performed with considerably less time and effort and with better control. This is better again in case of the BMS where a sample volume of only 0.5 l is required and experiments are performed in a controlled environment of a standard rheometer.

For a yield stress determination, the slump test is the simplest to apply, as it requires a sample volume of less than 1 l for fluids having $d_{max} = 10$ mm. Applying the test for fluids having $d_{max} = 25$ mm, a sample volume of approximately 20 l is necessary. In comparison, the capillary rheometer and the inclined plane test require sample volumes of 50 to 100 l for the yield stress determination of fluids having $d_{max} = 5$ to 10 mm. A further advantage of the slump test is that it can be applied relatively easily for low to highly concentrated fluids, or in a large range of the yield stress $\tau_y$, by using two complementary methods (slump height $S$ and profile of deposit). For the two other systems, this large range can be obtained only by adapting the experimental facility: In case of the inclined plane test, the inclination angle $i$ of the spreading plane or the sample volume must be increased, and in case of the capillary rheometer, larger capillaries or deeper cylinders/larger sample volumes would be necessary.

## Conclusions

The BMS implemented in a standard rheometer and requiring a sample volume of 0.5 l is an efficient tool for the rheological investigation of fluids containing particles from 0.25 to 10 mm grain size. Based on the model by Metzner and Otto (1957), the conversion of measured speed and torque data into rheological shear rate and shear stress data for Newtonian, power law, and yield stress fluids is derived. Robust coefficients of the shear stress and shear rate conversion were obtained for the laminar flow regime of the measuring sphere ($Re \leq 1$). In case of the yield stress fluids, it was shown that the coefficients correspond well with the yield stress criterion determining the onset of motion. For the transitional regime ($Re > 1$), the coefficients must be considered as a first estimation. This is because the different reference fluids did not indicate a unique behavior for a given fluid group, especially in case of the yield stress fluids. Future work must focus on testing and improving the coefficients by the investigation of additional fluids. However, the use of the derived coefficients is recommended.

In the second step, the flow curve and yield stress of large-particle fluids with variable maximum grain sizes $1 < d_{max} < 25$ mm were determined with the large-scale rheometer of Coussot and Piau, the BML viscometer, the BMS, a capillary rheometer, the inclined plane test, and the slump test and compared. Both the quality of the rheological data and fluid and device handling were considered. The flow curves of sediment–water mixtures from the first three rheometers could be determined within the same range of the shear stress $\tau$. This strengthens the reliability of these devices and the chosen methods for the conversion of measured into rheological data. Yield stress values usually did not differ by more than ±30% from the value obtained from the BMS, except for the capillary rheometer, where the yield stress deviation was usually considerably larger (+75%).

Despite the wide range of sample types and the very different experimental setting and procedure, all devices performed considerably well. This result strengthens the reliability of these rheometers except for the capillary rheometer. The remaining problems include the entry flow of the capillaries, particle segregation in the large-scale rheometer, the fully automated measuring procedure in the BML viscometer, and the slightly different readings for different sphere sizes in the BMS. In the latter case, this is assumed to be due to the variable length of the sphere holder and its variable distance from the container boundary depending on the used sphere.

The most crucial parameter in day-to-day use is the sample volume required for a specific apparatus or test. It governs experimental efficiency and control of fluid properties, such as sediment concentration and temperature. The BMS, the BML viscometer, and the slump test are preferred over all other systems. For the flow curve determination of fluids containing large particles with a maximum grain size $d_{max} = 1$ to 10 mm and with a maximum grain size $d_{max} = 5$ to 25 mm, the BMS and the BML viscometer are recommended, respectively. For the yield stress determination of fluids having $d_{max} < 25$ mm grain size, the slump test is recommended.

**Acknowledgement** Specials thanks are given to P. Coussot for his advice regarding the consolidation of the conversion theory in the laminar flow regime with the help of the yield stress criterion.

## Appendix: Problems encountered during BMS experiments

The basic experiment conducted with the BMS consists in measuring the torque $T$ at a given rotational speed $\Omega$ while the sphere makes one full rotation. Problems encountered during the measurement of particulated fluids with the BMS are tool acceleration, wake formation and viscous overstream, sphere interaction with suspended particles, data scattering due to grain size and temporary jamming, and the effect of prestructured samples. These problems are typical for many rheometrical measuring techniques and devices, but are considered below.

*Tool acceleration* In order to attain a specified rotational speed, the sphere must be accelerated, which requires an additional torque above that required to drag the sphere across a given fluid. Figure 15 shows the start-up flow for samples containing different maximum grain sizes and different sediment concentrations $C_v$. After acceleration, a steady drag flow around the sphere and sphere holder is achieved. In this regime, the measured torque is only dependent on the rheological properties of the fluid. Meaningful rheological data require steady-state flows, which must be established by experiments. As a consequence, only speed and torque data for the steady drag flow regime are used for any further rheological interpretation and for the conversion of measured into rheological data, respectively. Duration or number of data affected by the sphere acceleration regime primarily depends on the specified speed and, to a lesser extent, on the fluid characteristics. The influence of sphere acceleration is almost negligible for very small speeds but becomes very significant for high speeds. For example, for speeds equal to or larger than $\Omega = 2.25$ rps, the sphere acceleration regime covers one third up to half of the sphere path of a BMS experiment.

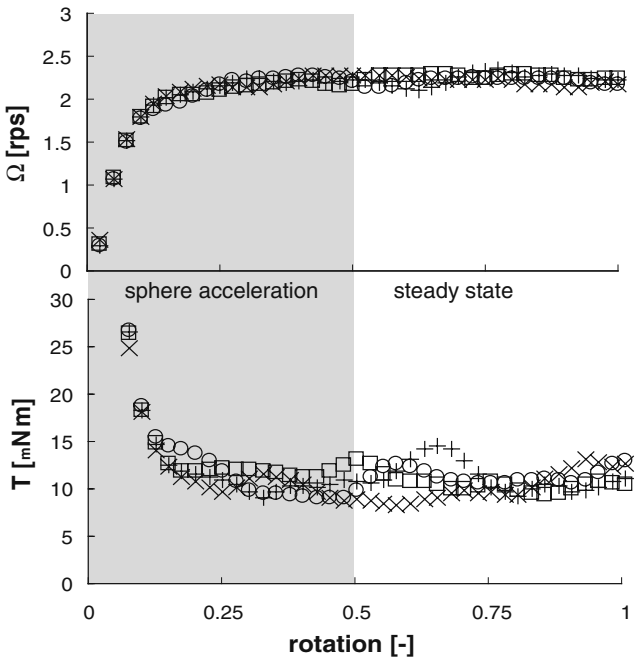


**Fig. 15** Basic BMS experiments using the sphere with the diameter $D = 12$ mm: development of the rotational speed $\Omega$ and the torque $T$ measured along the path of one sphere rotation for a specified speed of $\Omega = 2.25$ rps. **a** Sediment water mixture made of debris flow material with a maximum grain size $d_{max} = 1$ mm and a sediment concentration $C_v = 0.502$. **b** Maximum grain size $d_{max} = 10$ mm and a sediment concentration $C_v = 0.595$ [$C_v = V_s/(V_s + V_w)$ with $V_s$ = volume of sediment and $V_w$ = volume of the water]

*Wake formation and viscous overstream* In low viscous fluids (Newtonian or non-Newtonian, particulated or nonparticulated), it was observed that, for very high speeds of $\Omega = 2.25$–$4.5$ rps, the accelerating sphere generated a wake in front of the sphere and the sphere holder. For higher viscous fluids, such a wake was not observed. For silicon oils with viscosities larger than 2 Pa·s, the oil was lifted up along the sphere holder for higher rotational speeds. This was interpreted as viscous overstream ($\Omega \geq 1.35$ rps for the medium viscous oil, $\eta = 2$ Pa·s, $\Omega = 0.135$ rps in the case of the highly viscous oil $\eta = 60$ Pa·s). The measured torque might be biased due to this effect so that corresponding data should be interpreted with caution.

*Sphere–particle interaction, data scattering, and temporary jamming* The flow around the measuring sphere is ideally the flow of a homogeneous one-phase system. However, interactions of larger particles with the measuring sphere create a complex flow situation, in particular when both the suspended particles and the measuring sphere are of the same size (Chhabra 2007). Data fluctuation as seen for the different sphere diameters (see next chapter) are, however, related to the different geometries rather than to sphere–sphere interaction. Therefore, we have not considered the interaction of the moving sphere in the suspension.

*Data scattering and temporary jamming* Data fluctuation of both the rotational speed and the torque increases with an increasing maximum grain size $d_{max}$ of the particles for the steady drag flow regime (as shown in Fig. 15). For relative maximum grain sizes $d_{max}/D \leq 0.125$, the standard deviation of the speed $\sigma\Omega$ was typically less than 1% and, including fluctuation, remained

<4%. For the same range of the relative maximum grain size, the standard deviation of the torque $\sigma T$ was typically ~3% and, including fluctuation, remained <10%. A strong increase of the standard deviations, $\sigma T$ and $\sigma\Omega$, is observed for relative maximum grain sizes $d_{max}/D > 0.125$ and for fluids having $d_{max} \geq 5$ mm grain size. The standard deviation of the rotational speed, $\sigma\Omega$, not only depends on the relative maximum grain size $d_{max}/D$ but also strongly depends on the sediment concentration $C_v$ of the fluid (Fig. 16). For highly concentrated, large-particulated fluids, the standard deviation of the rotational speed $\sigma\Omega$ can thus attain values up to 100%. This behavior is mainly due to increasing friction and local or temporary jamming between the sphere, sphere holder, particles, and the container boundary along the sphere path, causing an increasing variation of the speed (Schatzmann et al. 2003b).

*Influence of prestructured sample* During the first full rotation, the sphere is dragged through an undisturbed sample fluid, whereas, for the following rotations, the sphere is dragged through a prestructured sample due to the influence of the first rotation, namely, along the sphere path. Depending on the value of the measured torque for the first and the following rotations at a given speed, it is, in principle, possible to determine whether or not the fluid is completely relaxed between the first and the following rotations and whether or not the fluid endured fatigue (Schatzmann 2005).

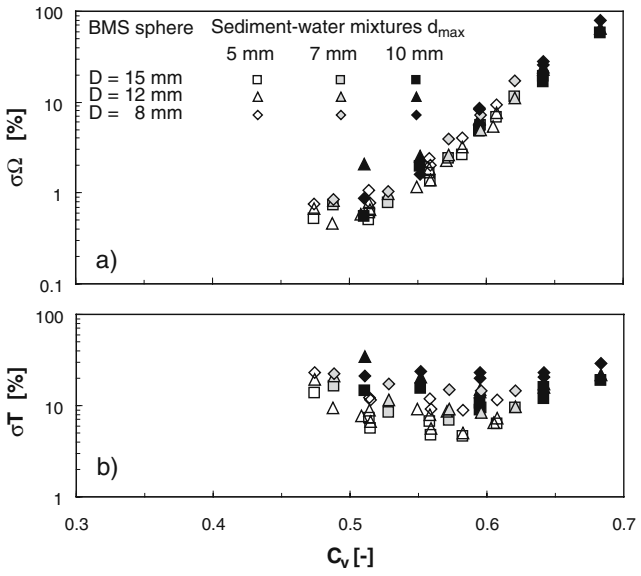


**Fig. 16** Standard deviation of the rotational speed, $\sigma\Omega$, and the torque, $\sigma T$, vs sediment concentration $C_v$ for sediment–water mixtures with variable maximum grain size $d_{max}$. Average standard deviation values obtained for $\Omega = 0.0045$, 0.0135, 0.045, 0.135, 0.45, 1.35, 2.25/2.7, and 4.5 rps

## Considerable side effects

The measuring sphere moves approximately at medium container depth through a sample fluid, which is at rest. Even though the sample fluid is stirred before every experiment, settling of particles may take place within measuring time. Although it is not expected that the settling particles influence the torque measurements, one must be aware of an inverse gradient of fluid concentration over the entire container depth. In fluids affected by particle settling, it is, thus, not clear whether at the sphere depth the rheological properties corresponding to the mean concentration of particles are measured.

The relatively small distances between the sphere and the container boundary (side and bottom), as well as the sphere holder, determine the drag flow and contribute to the total measured torque. The sphere holder is 0.6 mm thick and 3 mm long in the direction of the sphere path, and the immerged length varies between $s_i = 11$ mm for a $D = 15$-mm sphere and $s_i = 18$ mm for a $D = 8$-mm sphere. The distance between the container side and the sphere is $s_w = 17$ mm, and the distance between the container bottom and the sphere is $s_b = 22$ mm. While the influence of sphere holder and container boundary can be quantified for each sphere dragging across well-defined nonparticulated Newtonian fluids (Schatzmann 2005), some unpredictable effects remain when measuring in particulated Newtonian or non-Newtonian fluids.

One effect is, namely, the temporary transport of larger particles on top of the sphere while being supported backwards by the holder. In this case, the dragging body is not only the sphere and the holder but the sphere, the holder, and the large particle. As a consequence, increased torque values are measured in this case. A second effect is the temporary jamming of particles between the sphere, the container boundary, and/or the holder in high to highly concentrated mixtures producing relatively larger torque values. Both effects are difficult to assess based on the datasets of the torque and the speed in the steady drag flow regime because the effects are usually hidden behind the large data fluctuation in large-particulated fluids. One possibility to detect such an effect is the comparison of the torque data of two or several independent experiments performed at a specified speed. If the torque data of both experiments cover the same range, no such boundary effect is assumed to occur.

Another uncertainty is the influence of the container boundary on the yield stress fluids investigated in this study. The flow field of a sphere dragged across a yield stress fluid is characterized by a sheared zone around the dragged sphere and a nonsheared zone beyond the sheared zone (Beris et al. 1985; Chhabra and Uhlherr 1988). Generally, size and shape of the sheared zone depends on the sphere velocity, the parameters of the rheological model function of the fluid, and the confining boundary. Atapattu et al. (1995) measured size and shape of the sheared zone for spheres dragging across different yield stress fluids in tubes. Beaulne and Mitsoulis (1997) made numerical simulations and found a good agreement between the experimental data of Atapattu et al. (1995) and the numerical results. Based on the results of Beaulne and Mitsoulis (1997), the size of the sheared zone was estimated in the case of the present BMS. It was estimated that, for the different fluids and speeds investigated in the present study, the sheared zone must usually have spread to the container wall and bottom. This might not be the case for the small and medium spheres ($D = 8$, 12 mm) dragged at low velocities across the rather concentrated yield stress fluids. Because of the lack of appropriate technical equipment to measure the boundary of sheared and nonsheared zones in the present BMS device, this aspect was not further analyzed.

## References


Ancey C (2001) Role of lubricated contacts in concentrated polydisperse suspensions. J Rheol 45:1421–1439

Ancey C, Jorrot H (2001) Yield stress for particle suspension within a clay dispersion. J Rheol 45:297–319

Ansley RW, Smith TN (1967) Motion of spherical particles in a Bingham plastic. AIChE J 13:1193–1196

Atapattu DD, Chhabra RP, Uhlherr PHT (1995) Creeping sphere motion in Herschel–Bulkley fluids. J Non-Newton Fluid Mech 59:245–265

Banfill PFG (1994) Rheological methods for assessing the flow properties of mortar and related materials. Constr Build Mater 8:43–50

Banfill PFG, Beaupré D, Chapdelaine F, Larrard F, Domone P, Nachbaur L, Sedran T, Wallevik OH, Wallevik JE (2000) Comparison of concrete rheometers: international tests at LCPC (Nantes, France), NISTIR-Report 6819 of the NIST (National Institute of Standards and Technology)

Baudez JC, Chabot F, Coussot P (2002) Rheological interpretation of the slump test. Appl Rheol 12:133–141

Beaulne M, Mitsoulis E (1997) Creeping motion of a sphere in tubes filled with Herschel–Bulkley fluids. J Non-Newton Fluid Mech 72:55–71

Beris AN, Tsamopoulos JA, Armstrong RC, Brown RA (1985) Creeping motion of a sphere through a Bingham plastic. J Fluid Mech 158:219–244

Blackery J, Mitsoulis E (1997) Creeping motion of a sphere in tubes filled with a Bingham plastic material. J Non-Newton Fluid Mech 70:59–77

Borgia A, Spera FJ (1990) Error analysis for reducing noisy wide-gap concentric cylinder rheometric data for nonlinear fluids: theory and applications. J Rheol 34:117–136

Chhabra RP (2007) Bubbles, drop, and particles in non-newtonian fluids. Taylor & Francis, Boca-Raton

Chhabra RP, Richardson JF (1999) Non-newtonian flow in the process industries. Butterworth-Heinemann, Oxford

Chhabra RP, Uhlherr PHT (1988) Static equilibrium and motion of spheres in viscoplastic liquids. In: Cheremisinoff NP (Ed) Encyclopedia of fluid mechanics, vol 7. Gulf, Houston, pp 611–633

Clift R, Grace JR, Weber ME (1978) Bubbles, drops and particles. Academic, New York

Coussot P (2007) Plasticity and geophysical flows: a review. J Non-Newton Fluid Mech 142:4–35

Coussot P, Boyer S (1995) Determination of yield stress fluid behaviour from inclined plane test. Rheol Acta 34:534–543

Coussot P, Piau JM (1995) A large-scale field concentric cylinder rheometer for the study of the rheology of natural coarse suspensions. J Rheol 39:105–124

Coussot P, Proust S, Ancey C (1996) Rheological interpretation of deposits of yield stress fluids. J Non-Newton Fluid Mech 66:55–70

Coussot P, Laigle D, Arattano M, Deganutti A, Marchi L (1998) Direct determination of rheological characteristics of debris flow. J Hydraul Eng (ASCE) 124:865–868

Liu KF, Mei CC (1989) Slow spreading of a sheet of Bingham fluid on an inclined plane. J Fluid Mech 207:505–529

Major JJ, Pierson T (1992) Debris flow rheology: experimental analysis of fine-grained slurries. Water Resour Res 28:841–857

Metzner AB, Otto RE (1957) Agitation of non-newtonian fluids. AIChE J 3:3–10

Müller M, Tyrach J, Brunn PO (1999) Rheological characterization of machine-applied plasters. ZKG Int 52:252–258

Nguyen QD, Boger DV (1987) Characterization of yield stress fluids with concentric cylinder viscometers. Rheol Acta 26: 508–515

Nguyen QD, Boger DV (1992) Measuring the flow properties of yield stress fluids. Ann Rev Fluid Mech 24:47–88

Parsons JD, Whipple KX, Simoni A (2001) Experimental study of the grain-flow, fluid-mud transition in debris flows. J Geol 109:427–447

Pashias N, Boger DV, Summers J, Glenister DJ (1996) A fifty cent rheometer for yield stress measurement. J Rheol 40:1179–1189

Phillips CJ, Davies TRH (1991) Determining rheological parameters of debris flow material. Geomorphology 4:101–110

Roussel N, Coussot P (2005) "Fifty-cent rheometer" for yield stress measurements: from slump to spreading flow. J Rheol 49:705–718

Schatzmann M (2005) Rheometry for large particle fluids and debris flows. Dissertation No 16093, ETH Zurich, Zurich

Schatzmann M, Fischer P, Bezzola GR, Minor HE (2003a) The ball measuring system—a new method to determine debris flow rheology? In: Rickenmann D, Chen C (Eds) Proceedings of the 3rd international conference on debris flow hazards mitigation. Millpress, Rotterdam, pp 387–398

Schatzmann M, Fischer P, Bezzola GR (2003b) Rheological behaviour of fine and large particle suspensions. J Hydraul Eng (ASCE) 129:796–803

Schowalter WR, Christensen G (1998) Toward a rationalization of the slump test for fresh concrete: comparison of calculations and experiments. J Rheol 42:865–870

Schulze B, Brauns J, Schwalm I (1991) Neuartiges Baustellen-Messgerät zur Bestimmung der Fliessgrenze von Suspensionen. Sonderdruck aus Geotechnik 3/1991. Heidelberger Zement, Berliner Strasse 6, D-6900 Heidelberg

Shapley NC, Brown RA, Armstrong RC (2004) Evaluation of particle migration models based on laser Doppler velocimetry measurements in concentrated suspensions. J Rheol 48: 255–279

Tabuteau H, Coussot P, de Bruyn JR (2007) Drag force on a sphere in steady motion through a yield-stress fluid. J Rheol 51:125–137

Tattersall GH, Banfill PFG (1983) The rheology of fresh concrete. Pitman, London

Tattersall GH, Bloomer SJ (1979) Further development of the two-point test for workability and extension of its range. Mag Concr Res 31:202–210

Tyrach J (2001) Rheologische charakterisierung von zementären baustoffsystemen. Dissertation, Universität Erlangen-Nürnberg

Wallevik OH, Gjorv OE (1990) Development of a coaxial cylinder viscometer for fresh concrete. In: Proceeding of the rilem colloquium. Chapman and Hall, Hanover

Whipple KX (1997) Open-Channel flow of Bingham fluids: Applications in debris flow research. J Geol 105:243–262

Wilson SDR, Burgess SL (1998) The steady, spreading flow of a rivulet of mud. J Non-Newton Fluid Mech 79:77–85